Received: 31 August 2018 | Revised: 8 October 2018 | Accepted: 14 October 2018

DOI: 10.1002/aoc.4685

FULL PAPER

WILEY Applied Organometallic Chemistry

Organometallic ruthenium and iridium phosphorus complexes: Synthesis, cellular imaging, organelle targeting and anticancer applications

JuanJuan Li[1] | Zhenzhen Tian[1] | Shumiao Zhang[1] | Zhishan Xu[1,2] | Xudong Mao[1] | Yumin Zhou[1] | Zhe Liu[1]

[1]Institute of Anticancer Agents Development and Theranostic Application, The Key Laboratory of Life-Organic Analysis and Key Laboratory of Pharmaceutical Intermediates and Analysis of Natural Medicine, Department of Chemistry and Chemical Engineering, Qufu Normal University, Qufu 273165, China

[2]Department of Chemistry and Chemical Engineering, Shandong Normal University, Jinan 250014, China

Correspondence
Zhe Liu, Institute of Anticancer Agents Development and Theranostic Application, The Key Laboratory of Life-Organic Analysis and Key Laboratory of Pharmaceutical Intermediates and Analysis of Natural Medicine, Department of Chemistry and Chemical Engineering, Qufu Normal University, Qufu 273165, China.
Email: liuzheqd@163.com

Funding information
National Natural Science Foundation of China, Grant/Award Number: Grant No. 21671118; Taishan Scholars Program

The use of metal complexes containing phosphorus ligands as anticancer agents has not been well studied. In this work, eight novel half-sandwich Ir^{III} and Ru^{II} compounds with P^P-chelating ligands have been synthesized and fully characterized, and alongside two crystal structures were reported. All eight complexes displayed highly potent antiproliferative activity, up to nine times more potent than the clinical anticancer drug cisplatin towards A549 lung cancer cells. Complex **Ir1**, which has a simpler structure and highly potent antiproliferative activity, was selected to investigate in further mechanistic studies. No hydrolysis and nucleobase binding occurred for complex **Ir1**. In order to elucidate subcellular localization, the self-luminescence of the complex **Ir1** was utilized. **Ir1** can specifically target lysosomes and facilitate excessive production of reactive oxygen species, resulting in lysosomal membrane permeabilization in A549 cells. Release of cathepsin B and changes in the mitochondria membrane potential also contributed to the observed cytotoxicity of **Ir1**, which demonstrated an anticancer action mechanism that was different from that of cisplatin. The favorable results from biological and chemical research demonstrated that these types of complexes hold significant theranostic potential.

KEYWORDS
cellular imaging, cytotoxicity, lysosomes targeted, organometallic ruthenium and iridium phosphorus complexes

1 | INTRODUCTION

FDA-approved Pt-based agents (cisplatin, carboplatin and oxaliplatin) dominate conventional chemotherapy in a series of solid tumors, and are widely used in chemotherapy combinations.[1] However, only a small portion of the Pt-based drug can enter the body and form a biologically active form of platinum–DNA adducts, therefore these drugs have been limited by toxic side-effects (neurotoxicity, nephrotoxicity, myelosuppression, ototoxicity and vomiting), which are due to reaction with off-target nucleophiles, along with the fact that advanced patients rarely heal due to development of drug resistance during treatment.[2,3] To overcome these problems, metal complexes that differ from the anticancer mechanism of cisplatin have been designed by many research groups.[4–9] After platinum complexes, iridium (Ir) and ruthenium (Ru) complexes have displayed great potential

as novel metal-based anticancer drug candidates,[10–19] for example, NAMI-A and KP1019 are two Ru complexes that are already in clinical trials.[20,21]

Organelle targeting is essential for developing specific and effective cancer therapeutics, especially for chemotherapy.[22–24] Organelle targeting can increase drug concentration in its active form at the target where the drug works by delivering a drug to the cellular organelle, which may have the potential to increase efficiency and reduce side-effects.[25–28] Lysosomes targeting has emerged as an effective strategy in degrading compartments of the cell, including degrading proteins, membranes and other cellular organelles.[29] Complexes target lysosomes and then lysosomal membrane permeabilization (LMP) is increased, which causes cathepsins released from lysosomes to cytosol and initiate apoptosis. The increased LMP and subsequent cell death may be effective in cancer treatment, on condition that lysosomes of cancer cells can be the intended target.[30]

Metal complexes possessing O^O, O^N, and especially N^N-chelating ligands have been extensively studied;[31–38] however, complexes containing P^P-chelating ligands are still in their infancy.[39] Our previous work showed that half-sandwich complexes bearing BINAP as P^P-chelating ligand possess very promising anticancer properties; however, utilizing the self-luminescence of the complexes in elucidating subcellular localization and further explanations of the mechanism of anticancer properties were not explored.[40] Therefore, it is necessary to develop novel metal phosphorus complexes that not only possess organelle targeting strategies but also have high anticancer activity. To meet this goal, we synthesized a series of new Ir (III) and Ru (II) compounds including different P^P-chelating ligands (Figure 1). These complexes not only displayed potent antiproliferative activity, but also target specific lysosomes and cause damage to lysosomes. We also systemically studied their MoA, including nucleobase binding, cellular uptake mechanisms, lysosomal damage, cathepsin B release, apoptosis, reactive oxygen species (ROS), cell cycle, mitochondrial membrane potential (MMP) changes, and catalytic NADH analysis. We demonstrated that this class of complexes is attractive as novel bioimaging and anticancer agents.

2 | RESULTS AND DISCUSSION

2.1 | Syntheses and X-ray crystal structural analysis

2.1.1 | Syntheses

All the complexes were synthesized using an analogical procedure according to the reported method (Scheme 1).[40] All the complexes were characterized through ^{1}H-NMR spectra, elemental analyses (C, H and P) and mass spectroscopy (MS). A series of half-sandwich Ir^{III} pentamethylcyclopentadienyl and Ru^{II} arene complexes containing four diverse P^P-chelating ligands of the type $[(Cp^x/Arene)M(P^P)Cl]PF_6$, where M = Ir, Cp^x is pentamethylcyclopentadienyl (Cp*) or 1-biphenyl-2,3,4,5-tetramethyl cyclopentadienyl (Cp^{xbiPh}); M = Ru, arene is 2-phenylethanol-1-ol (bz-EA) and *p*-cymene (*p*-cym), and P^P is four different 1,2-bis (diphenylphosphino)-based chelating ligands were investigated. Eight half-sandwich iridium/ruthenium complexes **Ir1–Ir5, Ru1–Ru3** (Figure 1) were synthesized by the reactions between the ligands L1–L4 and the dinuclear iridium or ruthenium precursors dimer in methanol at ambient temperature. But the synthesis of part of the metal complexes was unsuccessful. All the complexes were newly synthesized and were isolated as PF_6 salts. The ^{1}H-NMR (500 MHz) spectra of complexes **Ir1–Ir5**, **Ru1–Ru3** are shown in Figures S6–S13.

2.1.2 | X-ray crystal structural analysis

During the preparation of the complexes, single crystals of $[(\eta^5\text{-Cp*})Ir(L3)Cl]PF_6$ (**Ir3**) and $[(\eta^6\text{-}p\text{-cym})Ru(L4)Cl]PF_6$ (**Ru3**) were grown from hexane/dichloromethane solution, and their structures were elucidated by X-ray crystallography. They are arranged in the monoclinic and triclinic crystal systems with the P2 (1), P-1 space groups, respectively. The asymmetric unit of **Ir3** and **Ru3** consists of a cation and hexafluorophosphate anions. Details of crystallographic data, selected bond lengths and angles with estimated standard deviations are listed in Tables 1 and 2. ORTEP diagrams are shown in Figure 2. The crystal structure determination showed that both complexes adopt the classical pseudo-octahedral three-legged piano-stool geometry. As for **Ir3**, the η^5-cyclopentadienyl ring displays the common π-bonded η^5-coordination mode, and the P^P ligands, occupying two coordination positions, occupy a bidentate chelate coordination mode (P^P). Finally, a chloride ion occupies the final site in the coordination sphere.

Compared with complexes contain the P^P-chelating ligand BINAP,[40] the distance between the centroid of η^5-Cp* or η^6-*p*-cym and the metal center (1.8824 Å, 1.7616 Å, respectively) in **Ir3** and **Ru3** are shorter, due to the comparatively weak trans effect of the ligands in **Ir3** and **Ru3**. It has been reported that the steric hindrance around the metal center was reflected by the bite angle in Cp*(P–P)MX.[39,41,42] **Ru3** exhibits a smaller bite angle than **Ir3** when comparing the bite angles P_1−M−P_2, P_1−M−Cl, and P_2−M−Cl. The two complexes of **Ir3** and **Ru3** have similar M−Cl and M−P bond distances.

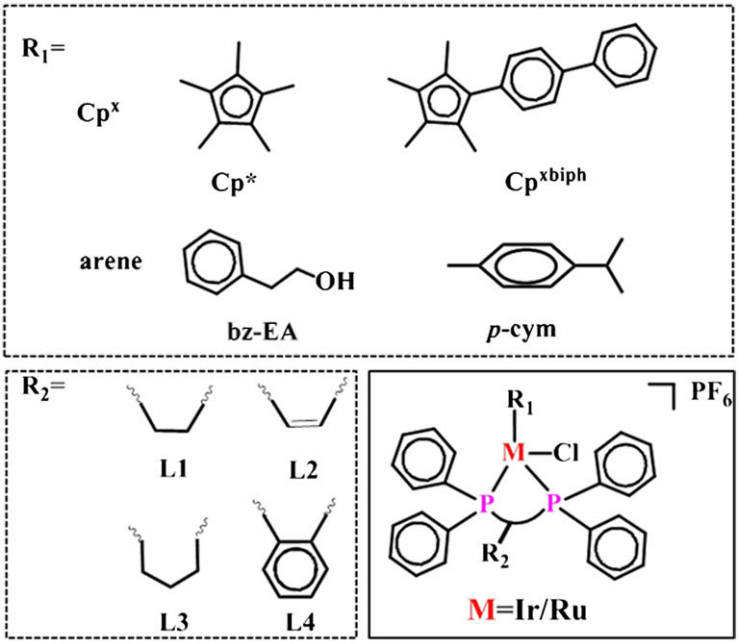

Complex	Cp^x / Arene	P^P
Ir1	Cp*	L1
Ir2	Cp*	L2
Ir3	Cp*	L3
Ir4	Cp^{xbiph}	L1
Ir5	Cp^{xbiph}	L2
Ru1	bz-EA	L1
Ru2	*p*-cym	L2
Ru3	*p*-cym	L4

FIGURE 1 Organometallic Ir^{III} cyclopentadienyl [(η^5-Cp^x)Ir(P^P)Cl]PF$_6$ and Ru^{II} arene [(η^6-arene)Ru(P^P)Cl]PF$_6$ complexes studied in this work

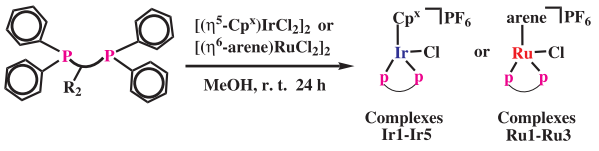

SCHEME 1 Synthesis of respective half-sandwich Ir^{III} and Ru^{II} complexes

2.2 | Cytotoxicity

The cytotoxicity of complexes **Ir1–Ir5**, **Ru1–Ru3** at various concentrations for 24 hr towards human cervical cancer HeLa and A549 human lung cancer cell lines was investigated by means of MTT assay. For the purposes of comparison, the toxicities and the IC_{50} (concentration where 50% of the cell growth is inhibited) values of cisplatin (CDDP) were also determined on the same cell lines, and the results are listed in Table 3. As shown in Table 3, the antiproliferative activity of the complex **Ir1** containing L1 is 3.4 × (towards A549 lung cancer cells) and 2.5 × (towards HeLa human cervical cancer) higher than the complex **Ir2** containing L2, showing a significant decrease in anticancer activity upon introduction of the vinyl group in L2. This trend is also exhibited between biphenyl complexes **Ir4** and **Ir5**. Adding a methylene group to L3 based on ligand L1, the anticancer

TABLE 1 Crystallographic data for $[(\eta^5\text{-Cp*})\text{Ir(L3)Cl}]PF_6$ (**Ir3**) and $[(\eta^6\text{-}p\text{-cym})\text{Ru(L4) Cl}]PF_6$ (**Ru3**)

	Ir3	Ru3
Formula	$C_{37}H_{41}Cl_3F_6P_3Ir$	$C_{40}H_{38}ClF_6P_3Ru$
MW	1005.52	862.13
Cryst. size (mm)	0.47 × 0.40 × 0.20	0.28 × 0.22 × 0.20
λ (Å)	0.71073	0.71073
Temp. (K)	293(2)	293(2)
Cryst. syst	Monoclinic	Triclinic
Space group	P2 (1)	P-1
a (Å)	13.2401(12)	11.097(2)
b (Å)	17.4358(15)	11.296(2)
c (Å)	26.194(2)	16.514(3)
α (°)	90.00	81.59(3)
β (°)	92.7920(10)	73.81(3)
γ (°)	90.00	86.05(3)
Vol. (Å^3)	6039.8(9)	1965.7(6)
Z	6	2
R1 [$I > 2\text{sigma}(I)$]	0.0699	0.0375
wR2 [$I > 2\text{sigma}(I)$]	0.1513	0.1042
GOF	1.062	1.058

TABLE 2 Selected bond lengths (Å) and angles (deg) for $[(\eta^5\text{-Cp*})\text{Ir(L3)Cl}]PF_6$ (**Ir3**) and $[(\eta^6\text{-}p\text{-cym})\text{Ru(L4)Cl}]PF_6$ (**Ru3**)

	Ir3	Ru3
M−C (cyclopentadienyl/arene)	2.193(13) 2.211(14) 2.246(17) 2.267(17) 2.297(15)	2.223(2) 2.223(2) 2.249(2) 2.262(2) 2.276(2) 2.310(2)
M−C (centroid)	1.8824	1.7616
$M-P_1$	2.330(4)	2.3046(8)
$M-P_2$	2.312(4)	2.3209(10)
M−Cl	2.405(4)	2.4005(9)
P_1-M-P_2	91.19(15)	83.48(3)
P_1-M-Cl	86.32(15)	81.54(4)
P_2-M-Cl	86.61(15)	84.45(3)

activity of complex **Ir3** is also reduced compared with that of complex **Ir1**. However, the anticancer activity of complex **Ru1** containing the P^P-chelating ligand L1 is lower than that of **Ir1** and **Ir4** containing L1, probably due to the hydrophilicity of −OH causing difficulties in entering the cell membrane.[43] A similar result has also appeared in our previous reports.[40] **Ru3** containing L4 is 2 × more active than **Ru2** containing L2 against HeLa human cervical cancer cells, suggesting that the introduction of a benzene ring on the ligand L2 can increase the anticancer activity of the complexes to some extent. When more benzene rings are added to the ligand L4 to form ligand BINAP, the anticancer activity of the corresponding η^6-*p*-cym ruthenium complex is further increased (IC_{50} from 5.6 to 1.4 μM).[40] Another striking result is that the biphenyl complex **Ir4** displayed lower IC_{50} values than the structurally similar Cp* derivative **Ir1**, and similar rules have been reported by Aird et al.[44] The results clearly indicate that subtle structural changes can have a significant impact on the antiproliferative activity. **Ir1** not only has a simpler structure but also has a relatively high anticancer activity against A549 lung cancer cells, and prompted us to further investigate the mechanism of action using **Ir1**.

The antiproliferative activities of the most potent complex **Ir1** were further evaluated against human bronchial epithelial normal cells 16HBE ($IC_{50} = 6.5 \pm 0.7$). Weak selectivity was observed between cancer cells vs. normal cells.

2.3 | Hydrolysis studies

Substitution of mono-ligand chloride by H_2O for metal complexes is a significant element influencing applications in medicine, such as activation of the Pt-Cl bond by $Pt\text{-}OH_2$ in cisplatin. In this study, the synthesized metal complexes have been dissolved using DMSO for NMR analysis and biological tests. Therefore, the hydrolysis of complex **Ir1** in DMSO/D_2O (3:7) was determined by ^{1}H-NMR at 37°C (Figure S1), and no change in the ^{1}H-NMR of the complex was observed during incubation for 24 hr, and was also unchanged after the addition of 16 × NaCl. The results suggest that hydrolysis did not occur under test conditions, and the intact metal complex is responsible for the observed cytotoxicity.

2.4 | Reaction with NADH

It is known that NADH (reduced nicotinamide adenine dinucleotide) and its oxidized form NAD^+ play a central role in mitochondrial function and cell death.[45] It has been reported that metal complexes can catalytically convert coenzyme NAD^+/NADH to produce ROS H_2O_2,[46] which can damage lysosomes and trigger the lysosomal pathway of apoptosis.[47] Therefore, the impact of **Ir1** (1 μM) on NADH (130 μM) was monitored in MeOH/H_2O (3:7) by UV–Vis at 298 K, and NADH was incubated in the same solution as control (Figure 3). The conversion from NADH to NAD^+ was determined

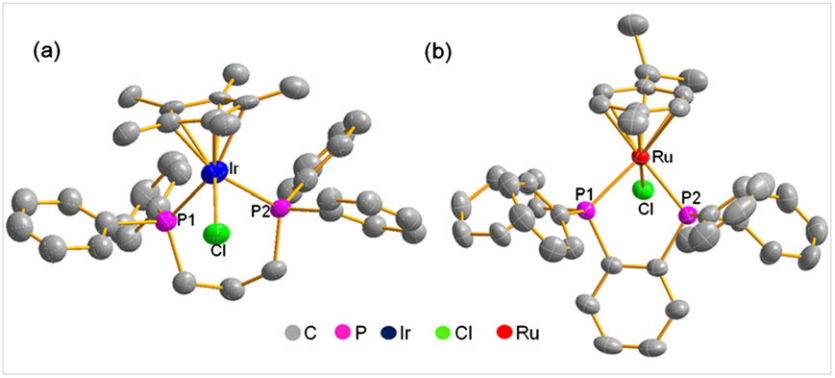

FIGURE 2 X-ray crystal structures with atom numbering schemes for (a) [(η^5-Cp*)Ir(L3)Cl]PF_6 (**Ir3**); (b) [(η^6-*p*-cym)Ru(L4)Cl]PF_6 (**Ru3**) with thermal ellipsoids drawn at 50% probability. The hydrogen atoms, dichloromethane and counter ions PF_6^- have been omitted for clarity

TABLE 3 Inhibition of growth of A549 and HeLa cancer cells by complexes **Ir1**–**Ir5**, **Ru1**-**Ru3** and comparison with cisplatin (CDDP) recorded over a period of 24 hr[a]

Complex	IC_{50} (μM) A549	HeLa	16HBE
[(η^5-Cp*)Ir(L1)Cl]PF_6 (**Ir1**)	3.0 ± 0.2	5.2 ± 0.6	6.5 ± 0.7
[(η^5-Cp*)Ir(L2)Cl]PF_6 (**Ir2**)	10.3 ± 0.6	12.9 ± 0.4	
[(η^5-Cp*)Ir(L3)Cl]PF_6 (**Ir3**)	3.9 ± 0.4	8.5 ± 0.5	
[(η^5-Cp^{xbiph})Ir(L1)Cl]PF_6 (**Ir4**)	2.3 ± 0.1	4.3 ± 0.9	
[(η^5-Cp^{xbiph})Ir(L2)Cl]PF_6 (**Ir5**)	7.4 ± 0.7	10.2 ± 0.6	
[(η^6-bz-EA)Ru(L1)Cl]PF_6 (**Ru1**)	32.9 ± 0.2	38.6 ± 1.1	
[(η^6-*p*-cym)Ru(L2)Cl]PF_6 (**Ru2**)	5.1 ± 0.5	7.9 ± 0.3	
[(η^6-*p*-cym)Ru(L4)Cl]PF_6 (**Ru3**)	5.6 ± 0.8	3.9 ± 0.7	
CDDP	21.3 ± 1.7	7.5 ± 0.2	

[a]Cells were treated with different concentrations of the iridium, ruthenium complexes and cisplatin for 24 hr. Cell viability was determined by the MTT assay, and data were calculated as described in the Experimental section. Data are presented as means ± SD obtained in at least three independent experiments.

based on NADH having a UV absorption at 339 nm but not NAD^+. The turnover number (TON) of complex **Ir1** (TON = 18) was calculated, suggesting that the complex has a strong catalytic ability to convert coenzyme NAD^+/NADH couple.

2.5 | Interaction with nucleobases

The principal mode of action of cisplatin is formation of covalent Pt–DNA adducts.[1] Therefore, the binding of model nucleobase 9-methyladenine (9-MeA) to complex **Ir1** was studied. 9-MeA (3 mM) was added to the solution of complex **Ir1** (1.0 mM) in DMSO/D_2O (3:7), and ^{1}H-NMR spectra were monitored at 310 K (Figure S2). No nucleobase adduct was formed detected by NMR and MS.

2.6 | Subcellular localization and mechanisms of cellular uptake

Toward elucidating the mechanism of action of **Ir1**, the localization of **Ir1** in A549 cells was monitored by confocal fluorescence microscopy (Figure 4). We used the Lys-specific fluorescent dye LTDR or mitochondria-specific probe MTDR tracker to perform co-incubation with **Ir1** in live A549 cells. As shown in Figure 4, an excellent

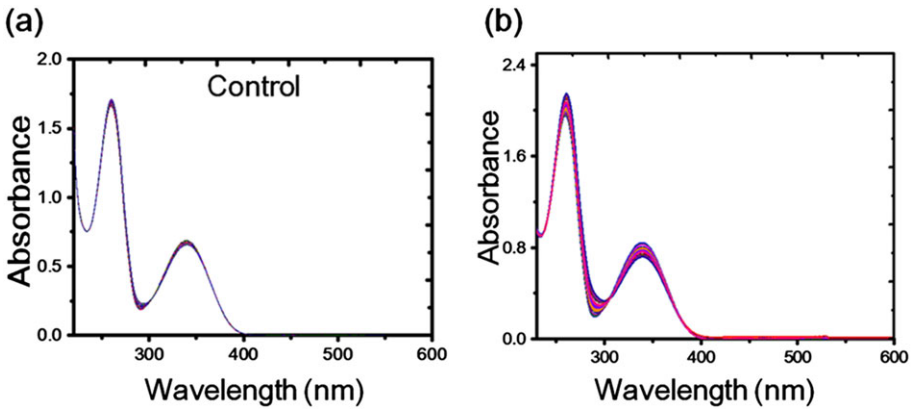

FIGURE 3 (a) UV–Vis spectra of the reaction of NADH (100 μM) in 30% MeOH/70% H_2O (V:V) at 298 K for 8 hr. (b) UV–Vis spectra of the reaction of NADH (130 μM) with **Ir1** (1 μM) in 30% MeOH/70% H_2O (V:V) at 298 K for 8 hr

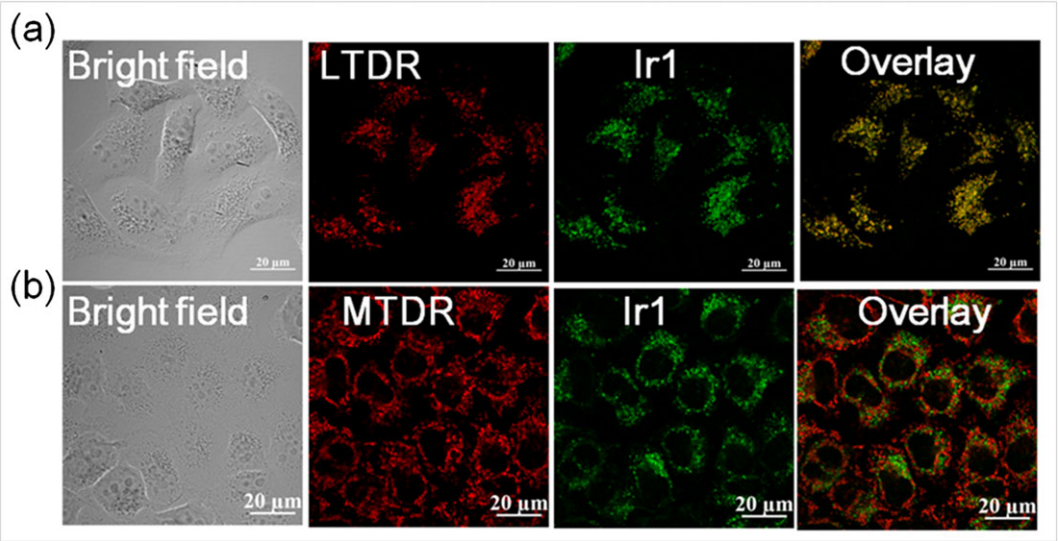

FIGURE 4 (a) Confocal microscopy images of A549 cells co-labeled with **Ir1** (10 μM, 0.5 hr) and LTDR (100 nM, 0.5 hr). (b) Confocal microscopy images of A549 cells co-labeled with **Ir1** (10 μM, 0.5 hr) and MTDR (75 nM, 0.5 hr). The excitation and emission bands for complex: $\lambda_{ex} = 488$ nm, $\lambda_{em} = 520 \pm 30$ nm; for MTDR: $\lambda_{ex} = 644$ nm, $\lambda_{em} = 700 \pm 30$ nm; for LTDR: $\lambda_{ex} = 594$ nm, $\lambda_{em} = 630 \pm 30$ nm. Scale bar: 20 μm

superimposition between the Lys-specific fluorescent dye LTDR and **Ir1** could be observed after incubating. The Pearson's *R*-value of colocalization is 0.92, demonstrating that most of the complex specifically targeted lysosomes. Meanwhile, minimal colocalization of **Ir1** with MTDR was observed. The Pearson's *R*-value of colocalization is 0.3. The results indicate that **Ir1** possesses lysosome targeting specificity. Lysosome plays crucial roles in a wide range of cell processes, including cell death.

Furthermore, to obtain more insight into the mechanism of the cellular entry of **Ir1**, we pretreated A549 cells with chloroquine, an endocytosis modulator that can inhibit the acidification of endosomes, the energy inhibitor CCCP (carbonyl cyanide *m*-chlorophenyl hydrazone) or incubation with **Ir1** at lower temperature (4°C), respectively (Figure S3), and cellular uptake efficiency was reduced as shown by confocal microscopy, indicating that cellular uptake of **Ir1** was mainly through an energy-dependent mechanism.

2.7 | Lysosomal damage and induction of intracellular ROS

2.7.1 | Lysosomal damage

The integrity of the lysosomes can be disrupted by metal complexes, which are well known to have a strong influence on promoting excessive generation of ROS and bringing about increased lysosomal permeability.[48,49] We incubated A549 cells with complex to evaluate the lysosomal integrity by acridine orange (AO, a very effective probe in studying the integrity of the acidic organelles) staining, which emits red fluorescence in lysosomes. As shown in Figure 5, A549 cells exposed to **Ir1** ($3 \times IC_{50}$) for 1 hr showed distinct red fluorescence in lysosomes. However, when the cells were incubated for 15 hr and 24 hr, the red fluorescence of AO arresting reduced in a time-dependent way, which manifested that lysosomes were seriously mangled.

The involvement of lysosomes and lysosomal proteases is seen as an extra point of turn into apoptosis in multifarious cell types. Disruption of the integrity of lysosomes can cause LMP (a crucial regulator of cell apoptosis), and promote cathepsin B released from lysosomes to cytosol. Cathepsin B Kit Magic Red was employed to detect the release of cathepsin B by confocal microscopy, and Hoechst 33342 was used to label the nuclei. Confocal microscopy displayed a dose-dependent augmentation in magic red fluorescence in A549 cells treated with **Ir1**. Compared with the control, an amount of cathepsin B was released in the present of **Ir1** at $3 \times IC_{50}$.

2.7.2 | Induction of intracellular ROS

Excessively produced ROS have been found to be an important component through a Fenton-like reaction to result in a more forthright influence on the lysosomal membrane, causing peroxidative damage to the membrane lipids, and leading to uncontrolled lysosomal permeability, along with modulation of apoptosis.[50] We further used fluorescent probe DCFH-DA, emitting green fluorescence upon oxidation by ROS, to measure the intracellular ROS

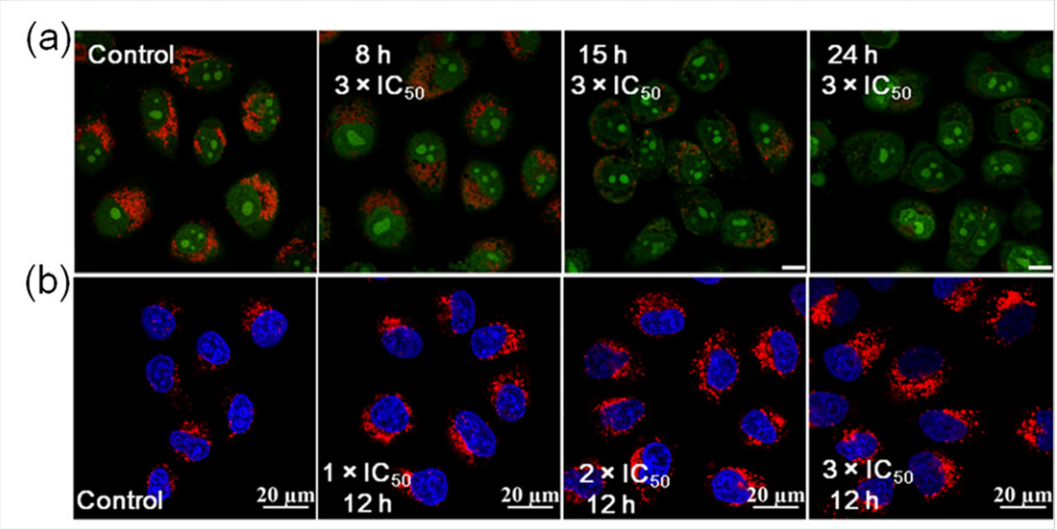

FIGURE 5 (a) Observation of lysosomal disruption in A549 cells caused by **Ir1** and stained by AO (5 μM, 15 min). λ_{ex} = 488 nm, λ_{em} = 510 ± 20 nm; λ_{em} = 625 ± 20 nm. The cells were treated with vehicle (1% DMSO), **Ir1** (9 μM) for 8 hr, **Ir1** (9 μM) for 15 hr, and **Ir1** (9 μM) for 24 hr, respectively. Scale bar: 10 μm. (b) Changes in cathepsin B location induced by different concentrations of **Ir1** for 12 hr in A549 cells using the fluorogenic substrate Magic Red MR-$(RR)_2$. Magic Red MR-$(RR)_2$ λ_{ex} = 543 nm, λ_{em} = 630 ± 20 nm. From left to right are vehicle (1% DMSO), **Ir1** 3 μM, **Ir1** 6 μM, **Ir1** 9 μM, respectively. Scale bar: 20 μm

level by flow cytometry analysis. As indicated in Figure 6 and Table S1 the ROS levels of A549 cells were very high even in the presence of a low concentration of **Ir1** ($0.25 \times IC_{50}$); **Ir1** exhibits excellent activity to generate ROS. These results demonstrated that **Ir1** could be used to induce oxidative damage and promote apoptosis.

2.8 | Apoptosis assay and MMP changes

Reactive oxygen species-intervened release of cathepsins, such as cathepsin B, takes place early during apoptosis, in advance of the loss of MMP.[47] Therefore, we performed a flow cytometric analysis to determine whether apoptosis and MMP reduction occurred. Firstly, apoptosis induced by **Ir1** was elucidated and analyzed by flow cytometric analysis. A549 cells were exposed to **Ir1** at 0.5, 1 and 2 equipotent concentrations of IC_{50} for 24 hr. As shown in Figure 7 and Table S2, a small portion of cells (12.1%) are in the apoptotic phase for control cells, and treating with complex decreases the percentage of cells in the viable phase dramatically, and a high apoptotic rate (65.8%) can be achieved for **Ir1** at $2 \times IC_{50}$. z-VAD-fmk (5 μM, pan-caspase inhibitor) was used to further

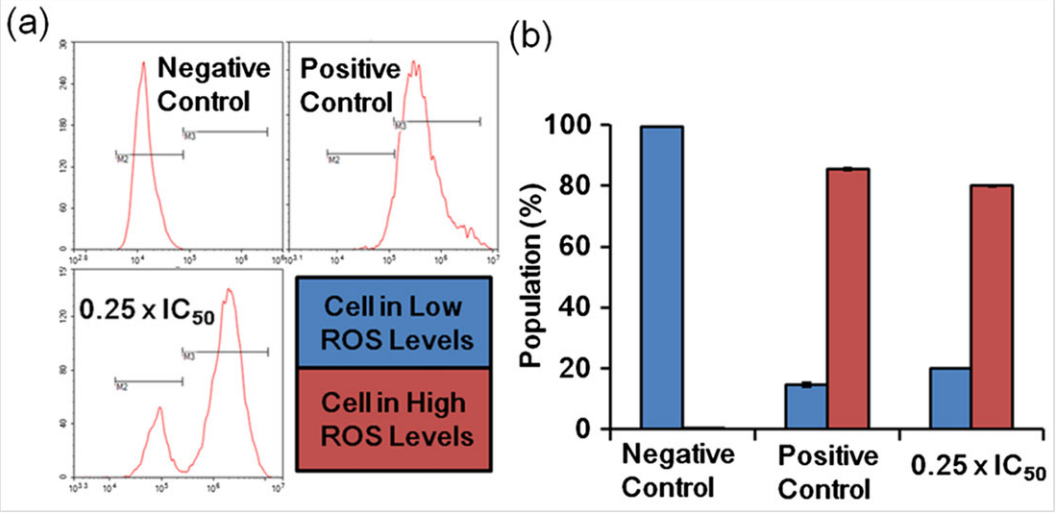

FIGURE 6 ROS induction in A549 cancer cells caused by complex **Ir1** at a concentration of $0.25 \times IC_{50}$. (a) FL2 histogram for negative control (untreated cells), positive control and **Ir1**. (b) Populations of cells in low and high levels of ROS after treatment of **Ir1**. Data are quoted as mean ± SD of three replicates

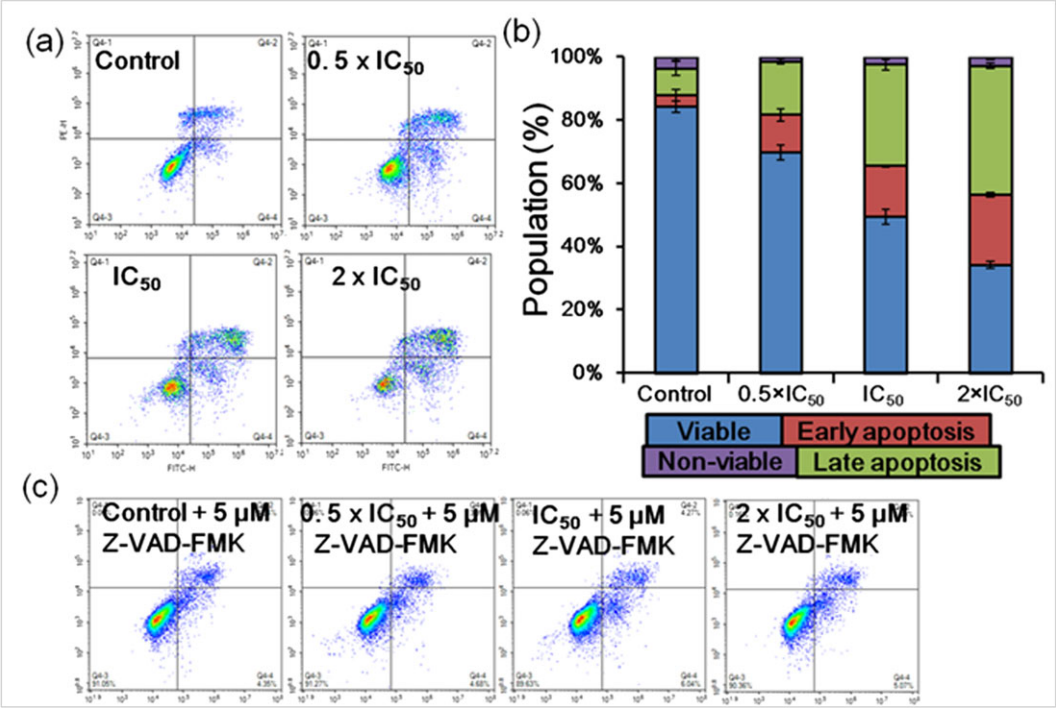

FIGURE 7 Flow cytometry detected the apoptosis based on annexin V and PI staining of A549 cells treated with different concentrations of complex **Ir1** after 24 hr at 310 K. The experiment was repeated three times, and representative photographs are displayed, with mean values of three independent experiments. Data are presented as mean ± S.D. (a) Populations for cells treated by **Ir1.** (b) Histogram for A549 cells treated with different concentrations of **Ir1** for 24 hr. (c) Populations for cells treated with different concentrations of **Ir1** and the pan-caspase inhibitor z-VAD-fmk (5 μM) at 310 K

evaluate the contribution of various caspases to apoptosis. The results showed that pretreatment of cells with z-VAD-fmk prevented cell apoptosis induced by **Ir1** significantly (Figure 7c; Table S3), revealing that apoptosis arose in a caspase-dependent manner.

Furthermore, JC-1 was exploited to study intracellular MMP dysfunction in A549 cells induced by **Ir1** (at concentrations of 0.25, 0.5, 1 and $2 \times IC_{50}$) using flow cytometry. Very recently, metal complexes have been used to attempt to induce cell apoptosis by interfering with the MMP, finally leading to cell death.[51,52] As shown in Figure S4 and Table S4, the increasing portion of green fluorescence confirmed that an increasing number of cells lost their MMP, when cells were treated with complex **Ir1**. MMP increased due to **Ir1**, probably due to the ROS generated leading to opening of the mitochondrial permeability transition pores and the release of cytochrome c (the biomarker of apoptosis).

2.9 | Cell cycle analysis

Platinum-based drugs, such as cisplatin, have been used to treat several forms of cancer mainly through forming types of platinum–DNA adducts, for example, the cytotoxicity of cisplatin was mediated via cisplatin–DNA adducts.[1,53] Therefore, we studied whether arresting the cell cycle was involved in cell death induced by complex **Ir1** using flow cytometric analysis. The A549 cells were exposed to **Ir1** at 0.25, 0.5 and $1 \times IC_{50}$ for 24 hr. Flow cytometric studies revealed that the percentages of cells in each cycle phase showed no significant change (Figure S5; Table S5), indicating that complex **Ir1** has no effect on the cell cycle, which digresses the pathway of the classical G_2/M arrest phase induced by cisplatin.[3] Therefore, we presumed that the correlation anticancer mechanism of action between complex **Ir1** and platinum-based drugs might be different.

3 | CONCLUSION

In conclusion, we presented the successful development of eight half-sandwich Ir^{III} and Ru^{II} complexes that reveal ligand changes lead to a significant impact on the cytotoxicity, and the P^P-chelating ligands are highly potent in enhancing antiproliferative activity. The metal complexes can specifically target to lysosomes and caused lysosomal damages in A549 cancer cells. The unearthing of the significant role of lysosome targeting specificity in cancer cells of half-sandwich metal complexes broadens our strategy for the design of more active anticancer

drugs. The significantly elevated excessive production of ROS and release of cathepsin B ultimately result in remarkable cytotoxicity, particularly in A549 human lung cancer cells lines, rather than the metal–DNA adduct mode of action similar to cisplatin. Flow cytometry studies have confirmed that the metal complexes induce apoptosis, especially late apoptosis, and changes in the MMP of cancer cells. The most detailed chemistry and biological studies points to the fact that metal complexes like **Ir1** can be very effective as anticancer drug candidates.

4 | EXPERIMENTAL

4.1 | General information

Unless otherwise noted, all manipulations were performed using standard Schlenk tube techniques under nitrogen atmosphere. The reagents $IrCl_3{\cdot}nH_2O$ (≥ 99% purity), hydrated $RuCl_3{\cdot}nH_2O$ (≥ 99% purity), octan-1-ol (≥ 99%) and nitric acid (72%), 2,3,4,5-tetramethyl-2-cyclopentenone (95%), 1,2,3,4,5-pentamethylcyclopentadiene (95%), butyllithium solution (1.6 M in hexane), 1,2-bis (diphenylphosphino) propare (98%), trans-1,2-bis (diphenylphosphino) ethylene (96%), 1,2-bis (diphenylphosphino) benzene (98%), 1,2-bis (diphenylphosphino) ethane (98%), 2-phenylethanol-1-ol (bz-EA) (98%), α-terpinene (*p*-cym) and cisplatin were purchased from Sigma-Aldrich. $Cp^{xbiph}H$[54] and $[(\eta^6\text{-bz-EA})RuCl_2]_2$[40] were prepared as described. For the biological experiments, CCCP, z-VAD-fmk and cleaved caspase-3 were purchased from Apoptosis and Epigenetice Company, NH_4PF_6 (Alfa Aesar), MTDR (Life Technologies), LTDR (Life Technologies), MTT [3-(4,5-dimethylthiazol-2-yl)-2,5–diphenyltetrazolium bromide] (Sigma-Aldrich), Annexin V-FITC Apoptosis Detection Kit (Sigma-Aldrich), JC-1 (Sigma-Aldrich), PBS (Sangon Biotech), PI (Sigma-Aldrich) were all used as received. DMEM medium, fetal bovine serum, penicillin/streptomycin mixture, trypsin/EDTA and PBS were purchased from Sangon Biotech. Testing compounds were dissolved in DMSO and diluted with the tissue culture medium before use.

4.2 | Synthesis of complexes Ir1–Ir5 and Ru1–Ru3

General method. The ligand 1,2-bis (diphenylphosphino) propare, trans-1,2-bis (diphenylphosphino) ethylene, 1,2-bis (diphenylphosphino) benzene or 1,2-bis (diphenylphosphino) ethane (0.10 mmol) and metal dimer $[(\eta^5\text{-Cp}^x)IrCl_2]_2$ or $[(\eta^6\text{-arene})RuCl_2]_2$ (0.05 mmol) were dissolved in methanol in a dry round-bottom flask equipped with room temperature stirrer and nitrogen atmosphere. NH_4PF_6 (0.2 mmol) was added after constant stirring for 12 hr. The reaction mixture was stirred for 6 hr at room temperature, and precipitate was formed in solution after complete conversion, methanol was removed under reduced pressure and product was dissolved in dichloromethane and filtered through Celite filtration funnel. Complexes were recrystallized by slow diffusion of *n*-hexane in a concentrated solution with complex in dichloromethane and the corresponding complexes (**Ir1–Ir5**, **Ru1–Ru3**) obtained.

4.2.1 | Synthesis of complexes Ir1–Ir5, Ru1–Ru3

$[(\eta^5\text{-Cp*})Ir(L1)Cl]PF_6$ (**Ir1**) reactant: 1,2-bis (diphenylphosphino) ethane (0.10 mmol) and metal dimer $[(\eta^5\text{-Cp}^*)IrCl_2]_2$. Yield: 34.1 mg, 37.6%. ^{1}H-NMR (500 MHz, DMSO-d_6): δ 7.70 (t, $^3J_{HH}$ = 7.6 Hz, 2H, CH_2), 7.63–7.46 (m, 11H, CH), 7.17 (s, 4H CH), 7.01 (s, 3H, CH), 1.49 (s, 2H, CH_2), 1.01 (s, 15H, Cp). Anal. calcd for $[(\eta^5\text{-Cp*})Ir(L1)Cl]PF_6$ (906.15): C, 47.71; H, 4.34; P, 10.25; found: C, 47.63; H, 4.31; P, 10.26. MS: m/z 726.22. $[(\eta^5\text{-Cp*})Ir(L1) + H]^+$.

$[(\eta^5\text{-Cp*})Ir(L2)Cl]PF_6$ (**Ir2**) reactant: trans-1,2-bis (diphenylphosphino) ethylene and metal dimer $[(\eta^5\text{-Cp}^*)IrCl_2]_2$. Yield: 29.4 mg, 32.5%. ^{1}H-NMR (500 MHz, DMSO-d_6): δ 7.72 (t, $^3J_{HH}$ = 7.5 Hz, 2H, CH), 7.56 (t, $^3J_{HH}$ = 7.2 Hz, 2H, CH), 7.45 (t, $^3J_{HH}$ = 7.7 Hz, 4H, CH), 7.36 (t, $^3J_{HH}$ = 7.6 Hz, 4H, CH), 7.21 (dd, $^3J_{HH}$ = 33.2 Hz, $^3J_{HH}$ = 14.1 Hz, 6H, CH), 6.86 (s, 4H, CH), 1.14 (s, 15H, Cp). Anal. calcd for $[(\eta^5\text{-Cp*})Ir(L2)Cl]PF_6$ (904.13): C, 47.82; H, 4.12; P, 10.28; found: C, 47.80; H, 4.11; P, 10.18. MS: m/z 724.20. $[(\eta^5\text{-Cp*})Ir(L2) + H]^+$.

$[(\eta^5\text{-Cp*})Ir(L3)Cl]PF_6$ (**Ir3**) reactant: 1,2-bis (diphenylphosphino) propare and metal dimer $[(\eta^5\text{-Cp}^*)IrCl_2]_2$. Yield: 27.5 mg, 29.9%. ^{1}H-NMR (500 MHz, DMSO-d_6): δ 7.60–7.46 (m, 8H, CH), 7.40 (q, $^3J_{HH}$ = 7.1 Hz, 8H, CH), 7.23 (dd, $^3J_{HH}$ = 10.9 Hz, $^3J_{HH}$ = 7.3 Hz, 4H, CH), 3.05 (d, $^2J_{HH}$ = 12.9 Hz, 2H, CH_2), 2.90 (dd, $^2J_{HH}$ = 11.1 Hz, $^3J_{HH}$ = 3.5 Hz, 2H, CH_2), 1.60 (dd, $^2J_{HH}$ = 16.2 Hz, $^3J_{HH}$ = 7.7 Hz, 2H, CH_2), 1.32 (s, 15H, Cp). Anal. calcd for $[(\eta^5\text{-Cp*})Ir(L3)Cl]PF_6$ (920.16): C, 48.29; H, 4.49; P, 10.10; found: C, 48.23; H, 4.39; P, 10.12. MS: m/z 740.23. $[(\eta^5\text{-Cp*})Ir(L3) + H]^+$.

$[(\eta^5\text{-Cp}^{xbiph})Ir(L1)Cl]PF_6$ (**Ir4**) reactant: 1,2-bis (diphenylphosphino) ethane (0.10 mmol) and metal dimer $[(\eta^5\text{-Cp}^{xbiph})IrCl_2]_2$. Yield: 29.9 mg, 28.6%. ^{1}H-NMR (500 MHz, DMSO-d_6): δ 7.66 (dd, $^3J_{HH}$ = 15.8, 8.4 Hz, 4H, CH), 7.63–7.47 (m, 12H, CH), 7.43 (ddd, $^3J_{HH}$ = 18.6 Hz, $^3J_{HH}$ = 12.0 Hz, $^3J_{HH}$ = 4.8 Hz, 5H, CH), 7.35 (d, $^3J_{HH}$ = 8.4 Hz, 2H, CH), 7.16 (dd, $^3J_{HH}$ = 11.5 Hz, $^3J_{HH}$ = 7.4 Hz,

4H, CH), 7.09 (d, $^3J_{HH}$ = 8.4 Hz, 2H, CH), 3.11–3.05 (m, 2H, CH_2), 2.72–2.65 (m, 2H, CH_2), 1.72 (s, 6H, Cp), 1.49 (s, 6H, Cp). Anal. calcd for [(η^5-Cp*)Ir(L1)Cl]PF_6 (1044.20): C, 54.05; H, 4.34; P, 8.90; found: C, 54.03; H, 4.31; P, 8.98. MS: m/z 864.27. [(η^5-Cp^{xbiph})Ir(L1) + H]$^+$.

[(η^5-Cp^{xbiph})Ir(L2)Cl]PF_6 (**Ir5**) reactant: trans-1,2-bis (diphenylphosphino) ethylene and metal dimer [(η^5-Cp^{xbiph})$IrCl_2$]$_2$. Yield: 28.9 mg, 27.7%. ^{1}H-NMR (500 MHz, DMSO-d_6): δ 7.78–7.74 (m, 2H, CH), 7.71 (d, $^3J_{HH}$ = 7.2 Hz, 2H, CH), 7.57 (d, $^3J_{HH}$ = 8.4 Hz, 2H, CH), 7.53–7.50 (m, 2H, CH), 7.46–7.30 (m, 9H, CH), 7.26–7.15 (m, 6H, CH), 7.07 (s, 4H, CH), 6.85 (s, 4H, CH), 1.48 (s, 6H, Cp), 1.29 (s, 6H, Cp). Anal. calcd for [(η^5-Cp^{xbiph})Ir(L2)Cl]PF_6 (1042.18): C, 54.15; H, 4.16; P, 8.91; found: C, 54.13; H, 4.11; P, 8.88. MS: m/z 862.25. [(η^5-Cp^{xbiph})Ir(L2) + H]$^+$.

[(η^6-bz-EA)Ru(L1)Cl]PF_6 (**Ru1**) reactant: 1,2-bis (diphenylphosphino) ethane (0.10 mmol) and metal dimer [(η^6-bz-EA)$RuCl_2$]$_2$). Yield: 24.5 mg, 30.5%. ^{1}H-NMR (500 MHz, DMSO-d_6): δ 7.68 (t, $^3J_{HH}$ = 7.6 Hz, 2H, CH), 7.54 (dt, $^3J_{HH}$ = 14.6 Hz, $^3J_{HH}$ = 7.1 Hz, 6H, CH), 7.46 (t, $^3J_{HH}$ = 7.6 Hz, 4H, CH), 7.28 (s, 3H, CH), 7.15 (s, 3H, CH), 6.04–5.98 (m, 2H, CH), 5.22 (s, 2H, CH), 4.72 (s, 1H, CH), 4.27 (t, $^3J_{HH}$ = 5.2 Hz, 1H, CH), 3.54 (s, 2H, CH_2), 2.90 (t, $^3J_{HH}$ = 10.9 Hz, 2H, CH_2), 2.20 (t, $^3J_{HH}$ = 6.0 Hz, 2H, CH_2), 2.02–1.94 (m, 2H, CH_2). Anal. calcd for [(η^6-bz-EA)Ru(L1)Cl]PF_6 (802.05): C, 50.91; H, 4.27; P, 11.59; found: C, 50.96; H, 4.31; P, 11.53. MS: m/z 622.12. [(η^6-bz-EA)Ru(L1) + H]$^+$.

[(η^6-*p*-cym)Ru(L2)Cl]PF_6 (**Ru2**) reactant: trans-1,2-bis (diphenylphosphino) ethylene and metal dimer [(η^6 -*p*-cym)$RuCl_2$]$_2$. Yield: 27.0 mg, 33.2%. ^{1}H-NMR (500 MHz, DMSO-d_6): δ 7.76–7.71 (m, 2H, CH), 7.57–7.53 (m, 2H, CH), 7.45 (dd, $^3J_{HH}$ = 10.3, 4.8 Hz, 8H, CH), 7.29 (s, 4H, CH), 7.11 (s, 4H, CH), 6.92–6.83 (m, 4H, CH), 6.21 (d, $^3J_{HH}$ = 6.0 Hz, 2H, CH), 5.19 (d, $^3J_{HH}$ = 6.1 Hz, 2H, CH), 1.21 (s, 3H, CH_3), 0.85 (d, $^3J_{HH}$ = 6.9 Hz, 6H, CH_3). Anal. calcd for [(η^6-*p*-cym)Ru(L2)Cl]PF_6 (812.07): C, 53.24; H, 4.47; P, 11.44; found: C, 53.23; H, 4.45; P, 11.48. MS: m/z 632.14. [(η^6-*p*-cym)Ru(L2) + H]$^+$.

[(η^6-*p*-cym)Ru(L4)Cl]PF_6 (**Ru3**) reactant: 1,2-bis (diphenylphosphino) benzene and metal dimer [(η^6 -*p*-cym)$RuCl_2$]$_2$. Yield: 31.7 mg, 36.8%. ^{1}H-NMR (500 MHz, DMSO-d_6): δ 7.92 (dd, $^3J_{HH}$ = 10.7 Hz, $^3J_{HH}$ = 7.5 Hz, 6H, CH), 7.70–7.66 (m, 2H, CH), 7.65–7.62 (m, 2H, CH), 7.58 (t, $^3J_{HH}$ = 7.3 Hz, 4H, CH), 7.53 (t, $^3J_{HH}$ = 7.4 Hz, 2H, CH), 7.38 (t, $^3J_{HH}$ = 7.4 Hz, 4H, CH), 7.06 (t, $^3J_{HH}$ = 9.1 Hz, 4H, CH), 6.34 (d, $^3J_{HH}$ = 6.1 Hz, 2H, CH), 6.29 (d, $^3J_{HH}$ = 6.3 Hz, 2H, CH), 2.40–2.36 (m, 1H, CH), 1.26 (s, 3H, CH_2), 0.71 (d, $^3J_{HH}$ = 6.9 Hz, 6H, CH_3). Anal. calcd for [(η^6-*p*-cym)Ru(L4)Cl]PF_6 (862.08): C, 55.72; H, 4.44; P, 10.78; found: C, 55.73; H, 4.41; P, 10.88. MS: m/z 682.15. [(η^6-*p*-cym)Ru(L4) + H]$^+$.

ACKNOWLEDGEMENTS

The authors thank the National Natural Science Foundation of China (Grant No. 21671118) and the Taishan Scholars Program for support.

CONFLICT OF INTEREST

The authors declare no competing financial interest.

ORCID

Zhe Liu https://orcid.org/0000-0001-5796-4335

REFERENCES

[1] D. Wang, S. J. Lippard, *Nat. Rev. Drug Discov.* **2005**, *4*, 307.

[2] Y. R. Zheng, K. Suntharalingam, T. C. Johnstone, H. Yoo, W. Lin, J. G. Brooks, S. J. Lippard, *J. Am. Chem. Soc.* **2014**, *136*, 8790.

[3] S. G. Awuah, Y. R. Zheng, P. M. Bruno, M. T. Hemann, S. J. Lippard, *J. Am. Chem. Soc.* **2015**, *137*, 14,854.

[4] Z. Liu, P. J. Sadler, *Acc. Chem. Res.* **2014**, *47*, 1174.

[5] Y. Jiang, X. Wang, D. Hu, *Cell Death Dis.* **2017**, *8*, 2815.

[6] E. Kahrović, A. Zahirović, S. Kraljević Pavelić, E. Turkušić, A. Harej, *J. Coord. Chem.* **2017**, *70*, 1683.

[7] J. X. Liang, H. J. Zhong, G. Yang, K. Vellaisamy, D. L. Ma, C. H. Leung, *J. Inorg. Biochem.* **2017**, *177*, 276.

[8] C. Licona, M.-E. Spaety, A. Capuozzo, M. Ali, R. Santamaria, O. Armant, F. Delalande, A. V. Dorsselaer, S. Cianferani, J. Spencer, M. Pfeffer, G. Mellitzer, C. Gaiddon, *Oncotarget* **2017**, *8*, 2568.

[9] F. X. Wang, M. H. Chen, Y. N. Lin, H. Zhang, C. P. Tan, L. N. Ji, Z. W. Mao, *ACS Appl, Mater. Inter.* **2017**, *9*, 42,471.

[10] V. Novohradsky, L. Zerzankova, J. Stepankova, A. Kisova, H. Kostrhunova, Z. Liu, P. J. Sadler, J. Kasparkova, V. Brabec, *Metallomics* **2014**, *6*, 1491.

[11] R. Guan, Y. Chen, L. Zeng, T. W. Rees, C. Jin, J. Huang, Z. S. Chen, L. Ji, H. Chao, *Chem. Sci.* **2018**, *9*, 5183.

[12] M. Ganeshpandian, M. Palaniandavar, A. Muruganantham, S. K. Ghosh, A. Riyasdeen, M. A. Akbarsha, *Appl. Organomet. Chem.* **2018**, *32*, 4154.

[13] D. L. Ma, C. Wu, W. Tang, A. R. Gupta, F. W. Lee, G. Li, C. H. Leung, *J. Mater. Chem. B* **2018**, *6*, 537.

[14] S. Thota, D. A. Rodrigues, D. C. Crans, E. J. Barreiro, *J. Med. Chem.* **2018**, *61*, 5805.

[15] G. Devagi, F. Dallemer, P. Kalaivani, R. Prabhakaran, *J. Organomet. Chem.* **2018**, *854*, 1.

[16] K. M. Knopf, B. L. Murphy, S. N. MacMillan, J. M. Baskin, M. P. Barr, E. Boros, J. J. Wilson, *J. Am. Chem. Soc.* **2017**, *139*, 14,302.

[17] L. Zeng, P. Gupta, Y. Chen, E. Wang, L. Ji, H. Chao, Z.-S. Chen, *Chem. Soc. Rev.* **2017**, *46*, 5771.

[18] Y. Han, Z. Tian, S. Zhang, X. Liu, J. Li, Y. Li, Y. Liu, M. Gao, Z. Liu, *J. Inorg. Biochem.* **2018**, *189*, 163.

[19] J. Hess, H. Huang, A. Kaiser, V. Pierroz, O. Blacque, H. Chao, G. Gasser, *Chem. Eur. J.* **2017**, *23*, 9888.

[20] J. M. Rademaker-Lakhai, D. van den Bongard, D. Pluim, J. H. Beijnen, J. H. M. Schellens, *Clin. Cancer Res.* **2004**, *10*, 3717.

[21] C. G. Hartinger, M. A. Jakupec, S. Zorbas-Seifried, M. Groessl, A. Egger, W. Berger, H. Zorbas, P. J. Dyson, B. K. Keppler, *Chem. Biodiversity* **2008**, *5*, 2140.

[22] L. Rajendran, H. J. Knölker, K. Simons, *Nat. Rev. Drug Discov.* **2010**, *9*, 29.

[23] H. Xia, G. Gu, Q. Hu, Z. Liu, M. Jiang, T. Kang, D. Miao, Q. Song, L. Yao, Y. Tu, H. Chen, X. Gao, J. Chen, *Bioconjugate Chem.* **2013**, *24*, 419.

[24] W. Ma, Z. Tian, S. Zhang, X. He, J. Li, X. Xia, X. Chen, Z. Liu, *Inorg. Chem. Front.* **2018**, *5*, 2587. https://doi.org/10.1039/C8QI00620B

[25] N. M. Sakhrani, H. Padh, *Drug Des. Devel. Ther.* **2013**, *7*, 585.

[26] Z. Feng, H. Wang, S. Wang, Q. Zhang, X. Zhang, A. A. Rodal, B. Xu, *J. Am. Chem. Soc.* **2018**, *140*, 9566.

[27] Z. Xu, D. Kong, X. He, L. Guo, X. Ge, X. Liu, H. Zhang, J. Li, Y. Yang, Z. Liu, *Inorg. Chem. Front.* **2018**, *5*, 2100.

[28] J. Liu, C. Jin, B. Yuan, X. Liu, Y. Chen, L. Ji, H. Chao, *Chem. Commun.* **2017**, *53*, 2052.

[29] U. Repnik, V. Stoka, V. Turk, B. Turk, *BBA Proteins Proteom.* **2012**, *1824*, 22.

[30] N. H. T. Petersen, O. D. Olsen, L. Groth-Pedersen, A.-M. Ellegaard, M. Bilgin, S. Redmer, M. S. Ostenfeld, D. Ulanet, T. H. Dovmark, A. Lønborg, S. D. Vindeløv, D. Hanahan, C. Arenz, C. S. Ejsing, T. Kirkegaard, M. Rohde, J. Nylandsted, M. Jäättelä, *Cancer Cell* **2013**, *24*, 379.

[31] A. Habtemariam, M. Melchart, R. Fernández, S. Parsons, I. D. H. Oswald, A. Parkin, F. P. A. Fabbiani, J. E. Davidson, A. Dawson, R. E. Aird, D. I. Jodrell, P. J. Sadler, *J. Med. Chem.* **2006**, *49*, 6858.

[32] Z. Tian, J. Li, S. Zhang, Z. Xu, Y. Yang, D. Kong, H. Zhang, X. Ge, J. Zhang, Z. Liu, *Inorg. Chem.* **2018**, *57*, 10,498.

[33] D. Kong, M. Tian, L. Guo, X. Liu, S. Zhang, Y. Song, X. Meng, S. Wu, L. Zhang, Z. Liu, *J. Biol. Inorg. Chem.* **2018**, *23*, 819.

[34] Y. Sun, J. Yu, X. Liu, C. Zhang, J. Cao, G. Li, X. Liu, Y. Chen, H. Huang, *Biomed. Pharmacother.* **2018**, *102*, 699.

[35] G. Gasser, I. Ott, N. Metzler-Nolte, *J. Med. Chem.* **2011**, *54*, 3.

[36] C. G. Hartinger, N. Metzler-Nolte, P. J. Dyson, *Organometallics* **2012**, *31*, 5677.

[37] Q. Du, L. Guo, M. Tian, X. Ge, Y. Yang, X. Jian, Z. Xu, Z. Tian, Z. Liu, *Organometallics* **2018**, *37*, 2880.

[38] J. Li, L. Guo, Z. Tian, M. Tian, S. Zhang, K. Xu, Y. Qian, Z. Liu, *Dalton Trans.* **2017**, *46*, 15,520.

[39] F. Zhang, J. Jia, S. Dong, W. Wang, C.-H. Tung, *Organometallics* **2016**, *35*, 1151.

[40] J. Li, M. Tian, Z. Tian, S. Zhang, C. Yan, C. Shao, Z. Liu, *Inorg. Chem.* **2018**, *57*, 1705.

[41] H. Guan, M. Iimura, M. P. Magee, J. R. Norton, K. E. Janak, *Organometallics* **2003**, *22*, 4084.

[42] F. Zhang, X. Xu, Y. Zhao, J. Jia, C. H. Tung, W. Wang, *Organometallics* **2017**, *36*, 1238.

[43] M. Ganeshpandian, R. Loganathan, E. Suresh, A. Riyasdeen, M. A. Akbarsha, M. Palaniandavar, *Dalton Trans.* **2014**, *43*, 1203.

[44] R. E. Aird, J. Cummings, A. A. Ritchie, M. Muir, R. E. Morris, H. Chen, P. J. Sadler, D. I. Jodrell, *Br. J. Cancer* **2002**, *86*, 1652.

[45] Y. Zhao, J. Jin, Q. Hu, H. M. Zhou, J. Yi, Z. Yu, L. Xu, X. Wang, Y. Yang, J. Loscalzo, *Cell Metab.* **2011**, *14*, 555.

[46] L. Zhe, R. C. Isolda, Q. Bushra, H. J. M. H. Abraha, N. P. E. Barry, A. M. Pizarro, G. J. Clarkson, P. Sadler, *Angew. Chem. Int. Edit.* **2014**, *53*, 3941.

[47] R. Blomgran, L. Zheng, O. Stendahl, *J. Leukocyte Biol.* **2007**, *81*, 1213.

[48] L. Liu, Z. Zhang, D. Xing, *Free Radical Biol. Med.* **2011**, *51*, 53.

[49] L. He, Y. Li, C. P. Tan, R. R. Ye, M. H. Chen, J. J. Cao, L. N. Ji, Z. W. Mao, *Chem. Sci.* **2015**, *6*, 5409.

[50] N. Li, L. Yu, J. Wang, X. Gao, Y. Chen, W. Pan, B. Tang, *Chem. Sci.* **2018**, *9*, 3159.

[51] L. Li, Y. S. Wong, T. Chen, C. Fan, W. Zheng, *Dalton Trans.* **2012**, *41*, 1138.

[52] V. Pierroz, T. Joshi, A. Leonidova, C. Mari, J. Schur, I. Ott, L. Spiccia, S. Ferrari, G. Gasser, *J. Am. Chem. Soc.* **2012**, *134*, 20,376.

[53] M. Galanski, M. A. Jakupec, B. K. Keppler, *Curr. Med. Chem.* **2005**, *12*, 2075.

[54] C. Wang, J. Liu, Z. Tian, M. Tian, L. Tian, W. Zhao, Z. Liu, *Dalton Trans.* **2017**, *46*, 6870.

SUPPORTING INFORMATION

Additional supporting information may be found online in the Supporting Information section at the end of the article.

How to cite this article: Li JJ, Tian Z, Zhang S, et al. Organometallic ruthenium and iridium phosphorus complexes: Synthesis, cellular imaging, organelle targeting and anticancer applications. *Appl Organometal Chem*. 2019;e4685. https://doi.org/10.1002/aoc.4685